A low energy ion source for electron capture spectroscopy

C. Tusche[1,a)] and J. Kirschner[1,2]
[1]*Max-Planck-Institut für Mikrostrukturphysik, Weinberg 2, 06120 Halle, Germany*
[2]*Naturwissenschaftliche Fakultät II, Martin-Luther-Universität Halle-Wittenberg, 06120 Halle, Germany*

(Received 9 April 2014; accepted 11 June 2014; published online 27 June 2014)

We report on the design of an ion source for the production of single and double charged Helium ions with kinetic energies in the range from 300 eV down to 5 eV. The construction is based on a commercial sputter ion gun equipped with a Wien-filter for mass/charge separation. Retardation of the ions from the ionizer potential (2 keV) takes place completely within the lens system of the sputter gun, without modification of original parts. For 15 eV He^+ ions, the design allows for beam currents up to 30 nA, limited by the space charge repulsion in the beam. For He^{2+} operation, we obtain a beam current of 320 pA at 30 eV, and 46 pA at 5 eV beam energy, respectively. In addition, operating parameters can be optimized for a significant contribution of metastable He^{*+} (2s) ions. © *2014 AIP Publishing LLC*. [http://dx.doi.org/10.1063/1.4884900]

I. INTRODUCTION

The interaction of particles with surfaces plays an important role in the field of surface science. In particular, during the collisions of slow ions with metal surfaces inelastic and elastic charge transfer between the surface and the projectile takes place at a distance of a few Ångstrøm. The pioneering work by Hagstrum *et al.*,[1,2] using single charged particles, showed that a major fraction of the incident ions are neutralized after scattering at the metal surface, emitting a number of electrons. In a very similar way, the de-excitation of metastable neutral atoms at a surface proceeds, depending on the work function of the surface, either by direct Auger electron emission, or by ionization and subsequent neutralization of the projectile.[3] Ion neutralization spectroscopy (INS) or metastable de-excitation spectroscopy then uses the kinetic energy distribution of the ejected electron as a particularly surface sensitive electron spectroscopy tool.

More general, during the neutralization of highly charged ions (HCIs) at a conductive surface, several electrons have to be exchanged between the metal surface and the projectile.[4] HCIs are ions where all, or almost all, electrons were removed from the neutral atom. A prototypical model system for the processes involved is the double charged helium ion, He^{2+}, where the removal of two electrons with a total ionization potential of 79.0 eV from the helium atom leaves only the α particle. This is the most simple multiple charged ion where all electrons were removed. Already for this relatively simple system, several mechanisms for the charge transfer from the metal to the ion have to be considered. For instance, capture of electrons into ground- or excited states can take place assisted by the emission of Auger electrons. Also, direct resonant transitions take place into states close to the vacuum, and fill the outer shells. This so called "hollow atoms" then are subject to subsequent relaxation steps.[5,6] The capture of two electrons into the singlet or triplet terms of He** is detectable by the energy of the auger electrons emitted during the relaxation, and was discussed as a local probe of spin polarization.[7] Related to the high surface sensitivity, interpretation of the results, however, is complicated by subtle changes to the surface electronic properties.[8]

In the static picture, the available energy for the emission of electrons equals the ionization potential of the primary particle. In contrast to this "potential emission," inelastic transfer of the kinetic energy of the ion can lead to "kinetic emission." In order to separate the elastic and inelastic neutralization processes it becomes important to control the kinetic energy down to values lower than the potential energy of the ions.[9]

In this paper, we present the design of an ion source for low-energy helium ions with controllable charge states, optimized for the study of the neutralization dynamics at a metal surface by means of electron spectroscopy. In principle, single and double charged ions can be produced using a commercial sputter ion gun. However, these ion guns typically operate at acceleration voltages of a few 100 V up to several kV. When a kinetic energy in the order of a few eV/q, q being the charge state, is required, the ions have to be decelerated before arriving at the target. As was shown by Popova *et al.*[10] using a commercial sputter ion gun, deceleration to energies of a few eV can be achieved rather easily by floating the complete ion gun assembly on a negative potential, whereby the high energy ions that leave the source are decelerated towards the sample. In order to achieve a better control over the beam parameters such as energy spread, impact angle, and focus spot size, we followed a different approach, such that the ions are decelerated inside the lens system. This has the additional advantage that no electrical fields are present in the room above the sample, that would interfere with the analysis of ejected electrons by spectroscopy methods. In order to keep the design as simple as possible, the existing lens system of the commercial sputter ion gun was reused for building the deceleration optics.

a)Electronic mail: tusche@mpi-halle.mpg.de

II. ION GUN DESIGN

A. Experimental setup

Similar to the approach in Ref. 10 we decided to base our ion source on a commercially available sputter ion gun (SPECS IQE 12/38). The ion gun itself consists of two parts, the ionizer and the focusing lens system with two cylindrical elements and x- and y-deflection plate pairs. In addition, the ion gun is available with a Wien-filter for mass over charge selection. The Wien-filter is normally installed in between the ionizer and the optics.

As the ion gun, in its original state, is operated in the energy range from 500 eV up to 5 keV, ions produced in the ionizer have to be decelerated to the desired energy, in the range from 5 eV to 300 eV. The deceleration takes place inside the cylindrical lens system, after the Wien-filter. The retarding ratio, $R = \frac{E_{pass}}{E_{kin}}$, defined as the ratio between the energy of the ions passing the filter, E_{pass}, and the final energy, E_{kin}, will be in the range between $R = 10$ and $R = 100$.

The mechanical design of the modified ion source is displayed in Fig. 1. The ionizer system together with the Wien-filter assembly and the U-shaped permanent magnet are insulated with respect to the vacuum chamber and float on a high potential up to 3 kV. Connections to the pumping system, as well as the gas inlet are connected through ceramic vacuum breaks. An additional ceramic break, including an electric feed-through and a cylindrical lens (see below), connects the floating assembly to the original ion lens system of the ion gun, mounted directly to the vacuum chamber.

Except for the ceramic breaks and the transfer lens, no modifications of original parts of the ion gun are required. We note however, that in addition to the setup shown in Fig. 1 care should be taken with respect to the mechanical support of the source, in order to prevent breakage of the ceramics.

The low energy ion source is mounted to an ultra high vacuum (UHV) chamber (base pressure $<5 \times 10^{-11}$ mbar). Either a W(110) or a W(100) single crystal is used as the target, prepared by standard procedures.[11] The angle of incidence, φ, measured between the surface plane and the ion beam, can be adjusted from grazing incidence ($\approx 0°$) to 90°. Retarding potential curves and mass spectra are obtained by measuring the total sample current at perpendicular ion incidence. In addition, secondary electrons emitted from the ion neutralization processes at the surface are detected using a hemispherical electron energy analyzer (PHOIBOS 150, SPECS).

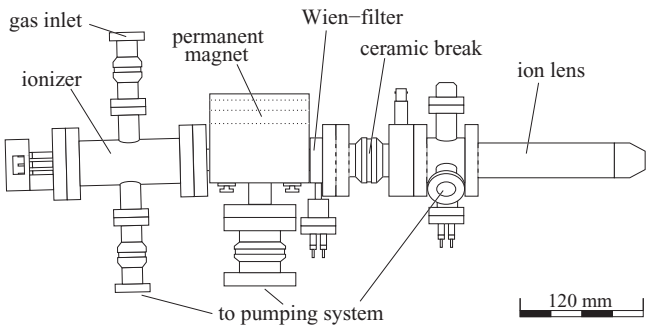

FIG. 1. Outline of the vacuum system of the low energy ion source.

B. Ion optics

In order to find an optimized retarding mode, ion trajectories were calculated using the SIMION[12] program package. As outlined above, the Wien-filter is connected to the original electrostatic lens system via a DN35 ceramic vacuum break. From the ion-optical point-of-view, a cylindrical electrode, L_0, floating on an intermediate potential connects the exit slit of the filter (A_1) to the original lens system with electrodes L_1 and L_2.

The result of the simulation for a retarding ratio $R = 100$ is displayed in Fig. 2(a). The horizontal scale is compressed, for clarity. Here, the ionizer potential is set to +20 V (with respect to ground) while the source potential is −1980 V, resulting in $E_{pass} = 2000$ eV or 4000 eV for He^+ or He^{2+} ions, respectively. The potential difference of 2 kV between the ionizer and source corresponds to the normal operating condition of the original sputter gun. In order to achieve the simulated configuration, the vacuum-housing of the ionizer and Wien-filter – electrically connected to the exit apertures of ionizer (A_0) and Wien-filter (A_1) in Fig. 2(a) – is floated on −1980 V with respect to ground.

The simulation shows trajectories originating from three points within the 1.8 mm diameter exit aperture of the ionizer, at the left side in Fig. 2(a). After passing through the mass

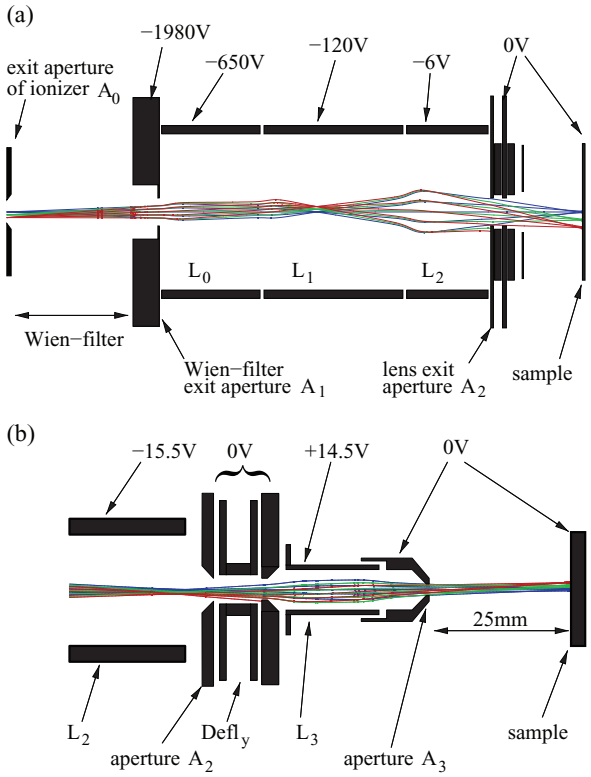

FIG. 2. (a) Calculated ion trajectories for retarding ratio $R = 100$ shown together with a schematic electrode layout. Ions start at the exit aperture of the ionizer, 120 mm left of the Wien-filter exit slit, with 2000 eV kinetic energy, and arrive at the sample with 20 eV kinetic energy. Blue, green, and red trajectories start at 0, 0.4, and 0.8 mm below the symmetry axis, respectively. Source potential and lens voltages are set as indicated. (b) The modified exit aperture, with the additional lens L_3 replacing the x-deflection plates. Labels indicate the electrode names and potentials. The working distance is reduced to 25 mm.

filter with E_{pass}, ions are decelerated in four steps by the electrode L_0, L_1, and L_2, set to negative voltages with respect to ground potential, as indicated in the figure. We note however, that for $R \approx 25$ zero crossing of the L_2 voltage is required. Deflection plates for the x- and y-directions located behind L_2, directly in front of the sample are not used, and connected to ground.

The first two deceleration steps at L_0 and L_1 correspond to a combined retarding ratio of ≈14, i.e., the kinetic energy in the center of L_1 is 140 eV/q. This high retarding ratio is connected with strong focussing of the ion beam, such that an intermediate gaussian image is formed in the center of L_1. The last lens element, L_2, is used to refocus the ion beam such that a second Gaussian image is located at the sample surface.

All potentials were optimized in order to obtain a high ion current density, i.e., a small beam diameter at the sample, and high transmission of the optics. For $R = 100$ we estimate a lower usable limit of the beam diameter of ≈4 mm, i.e., a magnification of 2:1 with respect to the exit aperture of the ionizer. From Fig. 2(a) it is evident that stronger focusing by L_2 will lead to a cut-off of outermost trajectories at the exit aperture, A_2 of the original lens system, owing to the large distance between L_2 and the sample. On the other hand, transmission is mainly limited by trajectories that cannot pass through A_2. Thus, transmission can be maximized by placing the second Gaussian image not at the sample, but close to the lens exit aperture and deflector assembly, at the cost of loosing a well defined focused beam spot at the sample.

It is therefore desirable to refocus the ion beam after the exit of the retarding lens, in order to combine a high transmission with a small beam diameter and a high current density. Figure 2(b) shows a modification of the exit of the ion optics. In order to overcome the limitations of the original design, an additional cylindrical lens, L_3, is introduced in front of the sample, replacing the (unused) x-deflection plates. In parallel, the working distance is reduced to 25 mm, and the aperture diameter is reduced to 2 mm. As displayed in Fig. 2(b) after deceleration by potentials L_0 through L_2 a second intermediate Gaussian image is formed in front of the aperture A_2 – which is the exit aperture of the retarding lens. No ion trajectories are cut off at this point, as the intermediate image is smaller than the aperture diameter. Focusing is always accomplished by a positive potential on L_3. From the simulation a unity magnification is estimated, i.e., we expect a beam diameter of ≈2 mm at the sample surface. The maximum beam divergence is limited by the diameter of the last aperture, A_3, which was chosen 2 mm, i.e., a beam divergence of $\approx \arctan \frac{2\,\mathrm{mm}}{25\,\mathrm{mm}} = 4.6^\circ$.

III. RESULTS

One critical parameter in the collision of ions with surfaces is the velocity of the projectile, i.e., the kinetic energy of the ions, intimately connected with the time scale and the trajectory above the surface. This is particularly important when using slow ions with kinetic energies of a few eV. As outlined above, the kinetic energy of ions arriving at the target crystal is set by the anode potential with respect to ground, multiplied by the charge state of the ion. Keeping the negative source potential fixed at ≈2 kV we measured the ion energy distribution by the total sample current in perpendicular incidence geometry.

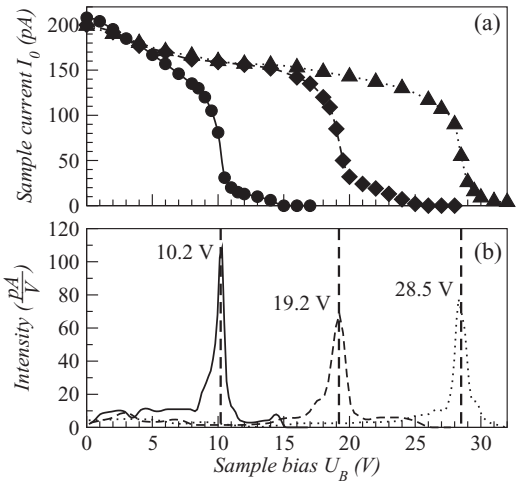

FIG. 3. (a) Total sample current versus retarding potential applied to the sample, measured using He^{2+} ions produced at an ionizer potential of 30 V (●), 40 V (♦), and 50 V (▲). (b) Ion energy distribution obtained from the retarding potential curves.

Figure 3(a) shows the sample current as a function of the positive retarding potential applied to the sample. The three curves correspond to an anode voltage of 30 V, 40 V, and 50 V, respectively. All curves exhibit a common slope on the low energy side of the spectrum. This is interpreted as the contribution of Auger- and secondary electrons emitted from the sample during the ion neutralization. The energy distribution of these electrons is fixed by the ionization potential of the charged particle, and independent of its kinetic energy.[5]

On the high energy side, the sample current rapidly drops to zero, indicating the maximum kinetic energy of the ions. The energy distribution displayed in Fig. 3(b) is obtained by numerical differentiation. We find a narrow peak with a full width a half maximum (FWHM) of about $1.2\frac{eV}{q}$, located ≈20 V below the anode potential. The difference can be interpreted as the amount of energy needed to extract an ion from the plasma inside the ionizer.

By contrast, for most filament-less ion sources, for instance electron-cyclotron-resonance (ECR) plasma sources, a positive value of the ion energy offset is observed. There, the sheath formed between the plasma and the walls leads to a positive plasma potential, which is typically in the order of some ten eV/q.[13] In the presence of a hot-cathode however, the effective potential at which the ions are created can be lowered compared to the potential of the ionizer due to electric field penetration form the cathode, and the buildup of a negative space charge. The negative offset of about −20 eV is in good agreement with values reported in Ref. 10 for the same type of ionizer.

In the example above, we used a beam of He^{2+} ions. Mass and charge selection is accomplished by the Wien-filter. As outlined above, ions pass through the filter with a high kinetic energy, before being decelerated. Inside the filter, ions move in a pair of crossed magnetic and electric fields. Ions with mass *m* will pass through the filter when the electrostatic

force and the Lorenz force which acts on the charged particle cancel out, and the ion moves along a straight line. This condition is fulfilled in the case of

$$\frac{m}{q} = 2 \cdot U_A \frac{B^2}{E^2}. \quad (1)$$

Here, m and q are the mass and the charge state of the ion, respectively, and the total acceleration voltage U_A corresponds to the kinetic energy by $U_A = \frac{E_{kin}}{e \cdot q}$. In the experiment, the magnetic flux density, B, is fixed by the permanent magnet, and the electric field, E, is adjusted in order to select the ion species.

Equation (1) shows that it is not possible to distinguish He^{2+} ions form H_2^+ ions, using the Wien-filter, as both species have the same mass over charge ratio, and a contamination of the He^{2+} beam by hydrogen cannot be ruled out completely. Therefore, we operate the ion source with ^3He gas instead of natural ^4He. (Without special notice, in the following He^+ and He^{2+} always refers to the ions of the ^3He isotope.)

Mass spectra are obtained by variation of the electrostatic deflection field in the Wien-filter. Figure 4 shows the measured sample current on a logarithmic scale as a function of the mass over charge ratio. Several contributions to the ion beam can be identified. As expected, the major contribution is the $^3He^+$ peak at $m = 3$ with a sample current of 29 nA. Double charged $^3He^{2+}$ is observed with a peak at $m = 1.5$ and a current of 0.33 nA. This corresponds to an efficiency for the production of double charged helium of about 1%, compared to single charged helium. Other ion species identified in Fig. 4 indicate contamination of the residual gas atmosphere inside the ionizer. The major contribution of the residual gas is hydrogen, i.e., the ion species H^+ and H_2^+ observed at mass $m = 1$ and $m = 2$, respectively.

Quantitatively, hydrogen contributes to the spectrum with about 15% of the $^3He^{2+}$ intensity. The contribution of the ^4He isotope to the spectrum can be measured by the intensity ratio $\frac{I(m=4)}{I(m=3)} = 0.04\%$, in agreement with the isotope ratio of the gas used. A significant contribution of $^4He^{2+}$ to the peak at $m = 2$

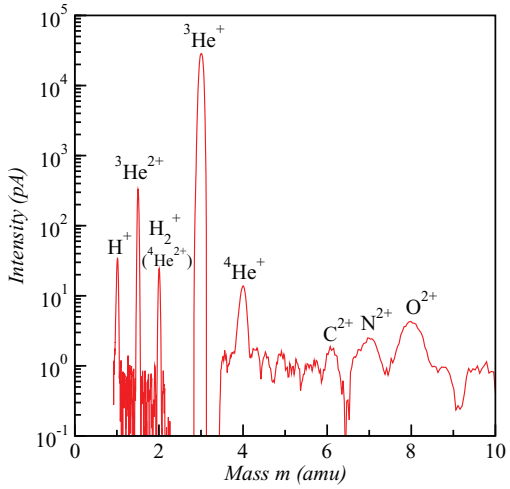

FIG. 4. Mass spectrum of ions leaving the source during operation with ^3He gas. The total sample current was measured at normal incidence using an ion energy of 15 eV/q and retarding ratio R = 100:1.

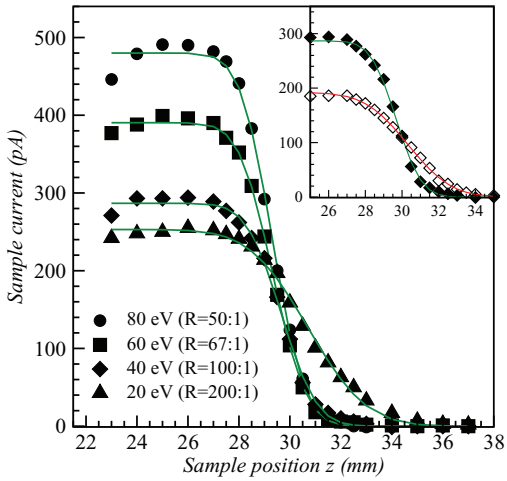

FIG. 5. Beam profile of 80 eV (•), 60 eV (■), 40 eV (♦), and 20 eV (▲) He^{2+} ions retarded from 4 keV pass energy. Solid lines show fits to a Gaussian profile with FWHM of 2.35 mm, 2.45 mm, 2.56 mm, and 4.27 mm, respectively. (Inset) 40 eV beam profile for the modified (solid symbols) vs. unmodified (open symbols) exit lens (FWHM = 4.41 mm).

therefore can be ruled out. For the production of a pure $^4He^{2+}$ beam a further reduction of the residual gas pressure inside the ionizer is advisable, which could be achieved either by prolonged operation and outgassing of the source, or a more efficient pumping system for hydrogen.

The current density distribution of the He^{2+} ion beam was derived by measuring the total sample current while moving the edge of the target crystal through the beam, using the z-translation of the manipulator. Figure 5 shows current profiles for He^{2+}ions with a kinetic energy of 80 eV, 60 eV, 40 eV, and 20 eV, using the modified exit lens from Fig. 2(b), including the additional focusing element L_3. In all cases, the pass energy was 4 keV, thus the ion optics was operated at a retarding ration of R = 50:1, 67:1, 100:1, and 200:1, respectively.

The curves have a step-like shape, which can be fitted by the error function, assuming a Gaussian beam profile. For the first three experiments, the fits result in a FWHM of 2.35 mm, 2.45 mm, 2.56 mm, respectively. This is in remarkably good agreement with the calculated beam diameter. For example, we expected a beam diameter of ≈2 mm for R = 100:1 (see Fig. 2(b)). It has to be pointed out though, that for higher retarding ratios like R = 200:1, and above, we could not find better focusing conditions than displayed in Fig. 5, with a FWHM of 4.27 mm.

The inset in Fig. 5 compares the beam profile for retarding ratio 100:1 and 40 eV kinetic energy, for the two geometries of the exit lens displayed in Figs. 2(a) and 2(b). Solid symbols show the data discussed above, obtained using the modified exit lens. In contrast, open symbols correspond to data measured with the original ion optics, without L_3. For the latter, we find a FWHM of 4.41 mm, which is significantly larger than for the optimized geometry. Looking at the ion trajectory simulations this is the expected result, however. Simultaneously, the total beam current increased from 200 pA to 300 pA, using comparable He-gas pressure in the ionizer. (The background pressure in the main chamber was reduced

from 1.6×10^{-8} to 5×10^{-9} mbar, due to the reduced diameter of the exit aperture, though.) In conclusion, adding the additional exit lens L_3 to the original ion optics of the sputter gun considerably increases the performance in terms of a four times increased current density and a reduction of the focal spot size from 4.4 mm to 2.6 mm.

The ion optical calculations did not include effects due to the space charge of the ion beam, so far. This is justified, regarding beam currents of some 100 pA for He^{2+} operation. However, it is well known that space charge induced broadening of the beam might become an issue for low energy ions.[14] For instance, we can consider a He^+ ion beam, where beam currents of 30 nA can be obtained (compare the peak at $m = 3$ in Fig. 4). Given the diameter of the exit aperture $d_0 = 2$ mm, the broadening Δd of a parallel ion beam can be approximated by Refs. 14 and 15,

$$\frac{\Delta d}{d_0} \approx \left(\frac{z}{d_0}\right)^2 \frac{1}{4\pi\epsilon_0}\sqrt{\frac{m}{2q\,e}}\,\frac{I}{U_B^{3/2}}, \tag{2}$$

where z is the distance from the exit aperture, ϵ_0 the dielectric constant, m and $q \cdot e$ the ion's mass and charge, I the beam current, and $U_B = \frac{E_{kin}}{q \cdot e}$ the beam voltage. Inserting values for 15 eV $^3He^+$ ions and 30 nA beam current (e.g., see Fig. 4) we obtain a typical broadening of $\Delta d/d_0 = 10\%$ for the geometry from Fig. 2(b). It is evident from Eq. (2) that space charge effects become dominant when higher beam currents or lower ion energies are desired.

The maximum beam current that can be obtained strongly depends on the acceleration voltage and the final kinetic energy of the ions. While a high pass energy, in general, favors a better extraction efficiency of the ions, it is accompanied by larger retarding ratios and reduced transmission of the decelerating optics. Figure 6 shows the beam current of He^{2+} ions as function of the kinetic energy on a double logarithmic scale. Individual curves were measured at constant pass energy, as indicated in the figure, i.e., by changing the retarding ratio.

Considerable He^{2+} beam currents were only obtained at pass energies above 2 keV, i.e., when the accelerating potential is above 1 kV. Increasing the pass energy to 3 keV further improves the ion current for the same E_{kin}. Higher pass energies do have no considerable influence on the beam current, therefore 3 keV represents the best working point for the source. When a small focus diameter is required, the results from Fig. 5 further suggest that the smallest possible retarding ratio should be chosen. We note that in addition to Fig. 5, where retarding ratios up to $R = 200{:}1$ were shown, the lowest kinetic energy measured in Fig. 6 was around 3.7 eV for He^{2+}, corresponding to $R = 800{:}1$. While the experiment shows that such low kinetic energies are possible to obtain at ion currents of a few 10 pA, no well defined beam profiles could be observed.

IV. OUTLOOK: ELECTRON SPECTROSCOPY

The performance of the ion source to produce well characterized beams of He^+ ions with a kinetic energy down to 5 eV, or He^{2+} ions with a kinetic energy down to 20 eV, makes it ideally suited for the studies of the electronic interactions between the valence electrons of the metal target and the projectile. We aim to analyze electrons emitted during the neutralization process that takes place while the slow ion is scattered at the single crystalline metal surface. The prototype process observed in "ion neutralization spectroscopy," as developed in the pioneering work by Hagstrum and Becker,[1,2] is the "Auger capture" of electrons to the 1s ground state of He^+. The excess potential energy ejects an Auger electron from the surface. As pointed out in Refs. 1 and 2, the obtained electron spectra are closely related to the self-convolution of the density of states involved in the neutralization process.

To this end, we show electron spectra measured during the neutralization of 5 eV He^+ ions at a clean W(100) single crystal in Fig. 7(a). The angle of incidence is set to 10° with respect to the target surface, and electrons are detected using the hemispherical analyzer at an emission angle of 60°

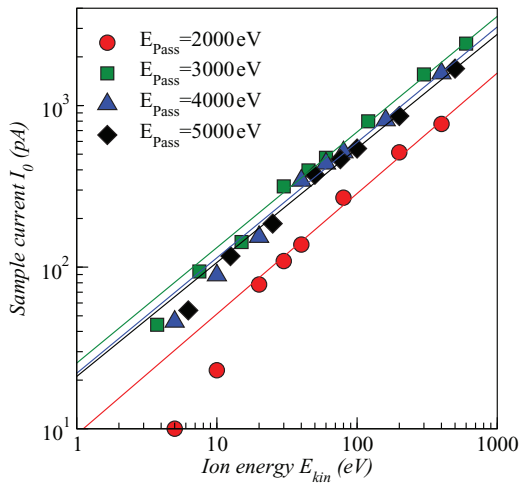

FIG. 6. He^{2+} ion beam current as function of the kinetic energy, measured for 2000 eV (●), 3000 eV (■), 4000 eV (▲), and 5000 eV (♦) pass energy. Solid lines serve as a guide to the eye.

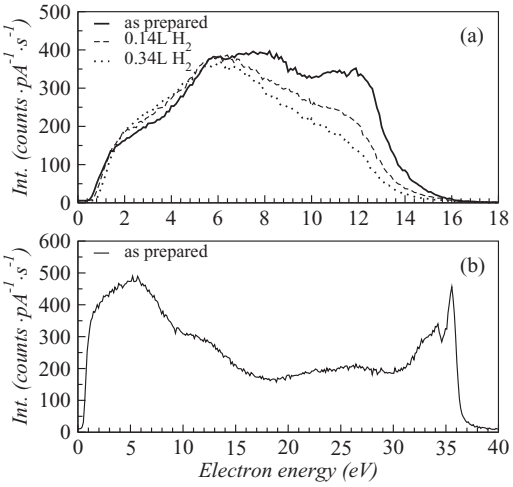

FIG. 7. (a) Energy spectrum of Auger electrons emitted in the neutralization of 5 eV He^+ ions at a clean W(100) surface, and after exposure to 0.12 L and 0.3 L of H_2. (b) Electron energy spectrum form the neutralization of 30 eV He^{2+} ions at a clean W(100) target.

$\pm$ 7.5° and energy resolution $\Delta E_{kin,e^-} = 0.2$ eV. The spectrum represented by the solid line was obtained immediately after preparation of the W(100) crystal. The procedure comprising several cycles of flashing (1700 K) in 5×10^{-8} mbar O_2 atmosphere, and a final high temperature (2500 K) flash removing the oxide layer, is known to lead to clean W(100) surfaces.[11] In addition, absence of surface reconstructions was checked by electron diffraction, and no traces of carbon or oxygen were detectable in Auger electron spectroscopy.

The overall shape of the spectrum of the clean surface is very similar to those published for nickel and copper surfaces in Ref. 2. The cut-off at about 15 eV is governed by the available potential energy, i.e., the ionization potential of free $He^+(1s)$ which is 24.6 eV, minus twice the work function of the surface. We demonstrate that the details of the electron spectra are particularly sensitive to the cleanliness of the surface. For instance, it is well known that tungsten single crystal surfaces are sensitive to adsorption of hydrogen from the UHV residual gas atmosphere.[16] In our experiments, the H_2 partial pressure during operation of the ion source is around 1.5×10^{-10} mbar, and the sample acquired a dose of 0.14 L (1 L = 1×10^{-6} Torr s) after 20 min and 0.34 L after 50 min, represented by the dashed and dotted curves in Fig. 7(a), respectively. Changes at the high energy side of the spectrum point out the exceptional surface sensitivity of the electron spectra.

In parallel, hydrogen adsorption on the W(100) surface results in a change of the work function, $\Delta\Phi$.[16] Compared to the clean sample, we find an increased work function by $\Delta\Phi = 0.16 \pm 0.05$ eV and 0.30 ± 0.05 eV for the exposure of 0.14 L and 0.34 L, respectively. For comparison, values reported in Ref. 16 are $\Delta\Phi \approx 0.15$ eV and 0.27 eV for the same H_2 doses.

Figure 7(b) shows the electron spectrum obtained for 30 eV He^{2+} ions. In contrast to Fig. 7(a), the spectrum extends to higher energies, up to ≈37 eV. Features in the spectrum account for the contribution of different neutralization channels.[17] For instance, sharp peaks around $E_{kin,e^-} = 34$ eV and 36 eV belong to the intra-atomic He-KLL Auger emission of metastable He** atoms formed above the surface.

As pointed out above, the neutralization of He^+ ions emits electrons with a maximum kinetic energy of about 15 eV. This allows us to separate the contribution of metastable $He^{*+}(2s)$ ions present in the beam. The electron configuration $He^{*+}(2s)$, i.e., one electron is the 2s shell, is stable with respect to radiative decay to the 1s ground state. At the target, electron capture leads to the formation of double excited He** with electron configuration $2\ell 2\ell'$ (with ℓ, ℓ' = s,p), similar to the neutralization of He^{2+}.[5]

However, the metastable $He^{*+}(2s)$ is quenched when passing through an electric field of some 100 V/cm due to the Stark effect.[18] In our experiment, electric fields inside the ionizer and the Wien filter are responsible for the quenching, when the pass energy is set too high. Figure 8 shows the yield of $He^{*+}(2s)$ ions, measured as the integrated number of electron counts in the energy range 30–38 eV and normalized to the total beam current, as function of the deflection field in the Wien filter. It is evident that for deflection fields above 320 V/cm no $He^{*+}(2s)$ is present in the beam, even though

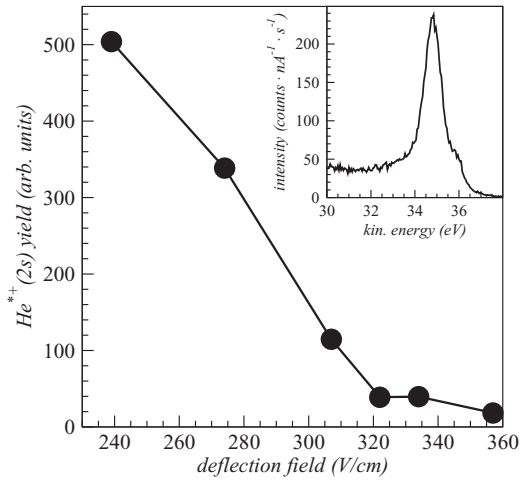

FIG. 8. He^{*+} (2s) yield versus electric field in the Wien filter, measured by the number of electrons emitted in the energy interval from 30 eV to 38 eV and normalized to the total sample current. (Inset) Normalized electron spectrum using 20 eV He^{*+} (2s) ions at the retarding ratio 10:1.

the total beam current was around 40 nA. For a low deflection field of 240 V/cm, i.e., at 200 eV pass energy, a reduced total beam current of 8 nA, but a largest possible fraction of metastable ions is obtained. The inset in Fig. 8 shows the corresponding electron spectrum of the He-KLL Auger line measured on a W(110) surface. Comparing the electron count rates with the He^{2+} spectra, we estimate that the fraction of metastable ions arriving at the target is around 1.3%.

V. DISCUSSION

A major difference in our design compared to the approach described in Ref. 10 is to keep the exit aperture of the electrostatic lens system at ground potential. This is achieved by electrical isolation using ceramic vacuum breaks between the original lens system and the ionizer, whereby the deceleration of ions takes place completely inside the lens system. By this design, the region around the sample is free of strong electric fields, in contrast to Ref. 10, where deceleration mainly takes place directly in front of the sample surface. The field-free sample environment is a prerequisite to study the emission of low energy electrons during the neutralization of the multiple charged ions by means of electron spectroscopy.

In addition, decelerating the ions inside the three-element lens system gives control over the beam focusing, verified by trajectory simulations. By using a Wien-filter for mass and charge separation it is possible to select a specific charge state of the ions. As demonstrated in our experiments, double charged helium is obtained at a fraction of ≈1% compared to single charged ions. While this results in beam currents of a few 100 pA for He^{2+}, other types of ionizers like electron cyclotron resonance,[19] or axial electron beam ionizers[20,21] are more efficient when higher charge states are desired. The setups typically also require a high acceleration voltage of several kV in order to extract the highly charged ions efficiently from the plasma. In principle, the retarding optics presented here could also be adapted to these kind of sources, when slow beams of HCIs with charge states larger than He^{2+} are required.

Using helium in particular, we showed that the operating parameters can be optimized towards a relatively large fraction of metastable $He^+(2s)$ ions in the beam, i.e., by both, a low acceleration voltage and retarding ratio. For instance, a direct comparison of the neutralization of He^{2+} and $He^{*+}(2s)$ in the same experiment could provide improved insight to the mechanism of the spin-dependent capture of two electrons from a surface, and the interpretation involved.[7,8] In contrast, operation at high acceleration voltages leads to a pure $He^+(1s)$ beam with no detectable (2s) contribution. This can be particularly useful for the selective investigation of different paths in the neutralization of the helium ions.

When the exit lens is used without modification, acceptable performance in terms of beam current and focus size can be obtained. In this configuration the source still can be used as a conventional sputter gun, when the ionizer housing is connected to ground. In this case, operation by the original power supplies is possible when the transfer lens L_0 is connected to L_1.

By replacing the exit aperture by a smaller one, and introducing an additional focusing lens (see Fig. 2(b)) in place of the x-deflection plates, the current density at the sample was increased by a factor of four. The original y-deflection plates are unused so far, and connected to ground. However, they could possibly be used for blanking the beam or generating short ion bunches by applying a differential voltage pulse.

In summary, we presented the design of an ion source optimized to produce a focused beam of ions with kinetic energies down to a few electron volts. The design is based on a commercially available mass filtered sputter gun, requiring only a minimal set of modifications. Due to the compact size, the source is ideally suited for the installation in surface analysis systems, dedicated to electron spectroscopy. Due to its outstanding surface sensitivity, INS could complement other techniques such as ultra-violet photoelectron spectroscopy. Special emphasis was put on the production of double charged, or metastable Helium ions, for the study of the physics of ion neutralization in vicinity of the target surface.

Moreover, we can imagine applications that cover the study of surface modifications by reactive or non-reactive ions, e.g., when an energy range in between thermal sources and classical sputter guns is required, or ion scattering experiments.

[1]H. D. Hagstrum, Phys. Rev. **150**, 495 (1966).
[2]H. D. Hagstrum and G. E. Becker, Phys. Rev. **159**, 572 (1967).
[3]G. Ertl, Philos. Trans. R. Soc. London A **318**, 51 (1986).
[4]J. Burgdörfer, P. Lerner, and F. W. Meyer, Phys. Rev. A **44**, 5674 (1991).
[5]H. D. Hagstrum and G. E. Becker, Phys. Rev. B **8**, 107 (1973).
[6]H. Winter and F. Aumayr, J. Phys. B: At. Mol. Opt. Phys. **32**, R39 (1999).
[7]M. Unipan, A. Robin, R. Morgenstern, and R. Hoekstra, Phys. Rev. Lett. **96**, 177601 (2006).
[8]M. Busch, S. Wethekam, and H. Winter, Phys. Rev. A **78**, 010901(R) (2008).
[9]P. Varga, Appl. Phys. A **44**, 31 (1987).
[10]I. Popova, R. Muha, Z. Chen, and J. T. Yates, Jr., J. Vac. Sci. Technol. A **21**, 401 (2003).
[11]K. Zakeri, T. Peixoto, Y. Zhang, J. Prokop, and J. Kirschner, Surf. Sci. **604**, L1 (2010).
[12]D. A. Dahl, Int. J. Mass Spectrom. **200**, 3 (2000).
[13]P. R. Harris and F. W. Meyer, Rev. Sci. Instrum. **81**, 02A310 (2010).
[14]H. Kawakatsu, K. Shimizu, and K. Kanaya, J. Electron Microsc. **18**, 111 (1969).
[15]K. T. Dolder and O. Klemperer, J. Appl. Phys. **26**, 1461 (1955).
[16]H.-J. Herlt and E. Bauer, Surf. Sci. **175**, 336 (1986).
[17]H. Brenten, H. Müller, and V. Kempter, Surf. Sci. **274**, 309 (1992).
[18]I. B. E. Nemirovsky and N. F. Freschi, J. Phys. B: At. Mol. Phys. **15**, 2579 (1982).
[19]Z. Q. Xie, Rev. Sci. Instrum. **69**, 625 (1998).
[20]G. Zschornack, M. Kreller, V. P. Ovsyannikov, F. Grossman, U. Kentsch, M. Schmidt, F. Ullmann, and R. Heller, Rev. Sci. Instrum. **79**, 02A703 (2008).
[21]M. Schmidt, H. Peng, G. Zschornack, and S. Sykora, Rev. Sci. Instrum. **80**, 063301 (2009).